Proceedings of 24th ASME/AIChE National Heat Transfer Conference, 1987

SMALL AMPLITUDE KINEMATIC WAVE PROPAGATION IN TWO-COMPONENT MEDIA

H.K. Kytömaa* and C.E. Brennen
Department of Mechanical Engineering
California Institute of Technology
Pasadena, California 91125

ABSTRACT

The speed and attenuation of small amplitude kinematic waves were measured in vertical bubbly and particulate flows in a continuous medium of water. This was done by evaluating the time delay and phase lag of coherent random fluctuations in the volume fraction signal at two measuring locations. The volume fraction was monitored using two closely spaced Impedance Volume Fraction Meters (Kytömaa (1986)). Using the broad-band volume fraction perturbations yields the dependence of the kinematic speed and attenuation on wave number from a single experiment for one set of conditions. The kinematic waves were found to be non-dispersive. Bubbly flows are observed to undergo a change in flow regime at an approximate volume fraction of 45%. Prior to onset o churn-turbulence, a sharp drop in kinematic wave attenu ation is observed above volume fractions of 40%. When further increase in volume fraction is attempted, the hc mogeneous dispersion suddenly becomes unstable. Th particulate flows remain uniformly dispersed for all vo ume fractions, but above a value of $\approx$ 55%, the mixtu flows like a solid plug. The volume fraction fluctuatio become increasingly persistent as the volume fraction a proaches the solidification value, but no instability is o served. It is argued that the inability of air-water flows to withstand bubble-bubble forces without break-up may account for the differences between the bubbly and particulate flow results.

1. INTRODUCTION

The departure of a two-component flow from the uniform dispersion of its constituents is known to be a major cause of inefficient fluidized bed operation (Homsy & al (1980), Anderson & Jackson (1967 & 1968), Zenz (1971)). It is also believed to be responsible for increased settling rates in liquid suspensions, as shown by Batchelor (1986), Fessas and Weiland (1981) and Whitmore (1955). The growth of small perturbations in the local concentration of particles is believed to be the source of such non-uniformities. The growth of structure in sedimenting two-particle mixtures of zero net flow has been studied by Batchelor and Fessas & Weiland. Their work uncovered the complex streaming as well as globular nature of the structure in bi-disperse systems. Didwania & Homsy (1981) studied the behavior of mono-disperse solid-liquid mixtures in two-dimensional fluidized beds, and observed the break down of initially planar concentration waves into two-dimensional structure. In this study, we focus on the nature of one-dimensional two-component flows. The propagation and growth of concentration waves is studied in flowing mixtures of inter-

: based on the relative velocity
s. the speed and attenuation
natic waves were measured in
bly and particulate flows in a
ater. This could have been be
rbation of known size in volume
ion and following its evolution
ach is limited by the difficulty
ottling the disperse medium to create small amplitude perturbations. Alternately, naturally occurring random fluctuations in volume fraction can be used as the perturbations of which the speed and growth rate are sought. This is the method used to obtain the dispersion relation for kinematic waves. For this, the "noise" in the volume fraction signals at two closely spaced locations was used to obtain the wave speed and attenuation of coherent volume fraction fluctuations.

file name
KYT078

2. EXPERIMENTAL FACILITY

The Three Component Flow Facility (TCFF) shown in Figure (1) was used to study small amplitude kinematic wave propagation in bubbly and particulate two-component flows. The test section is a vertical clear

* Present address: Department of Mechanical Engineering, Massachusetts Institute of Technology, Cambridge, Massachusetts 02139. Telephone: (617) 253-0006

acrylic pipe .1016 meters (4 inches) in diameter and 2.2 meters in length. The air- water flows are formed by introducing the gas through an injector situated inside the vertical pipe, .5 meters below the test section. The injector consists of an array of twelve 3.2 mm (1/8 inch) diameter brass tubes perforated with .4 mm (1/64 inch) holes. An 8 atm (120 psi) compressed air line supplies

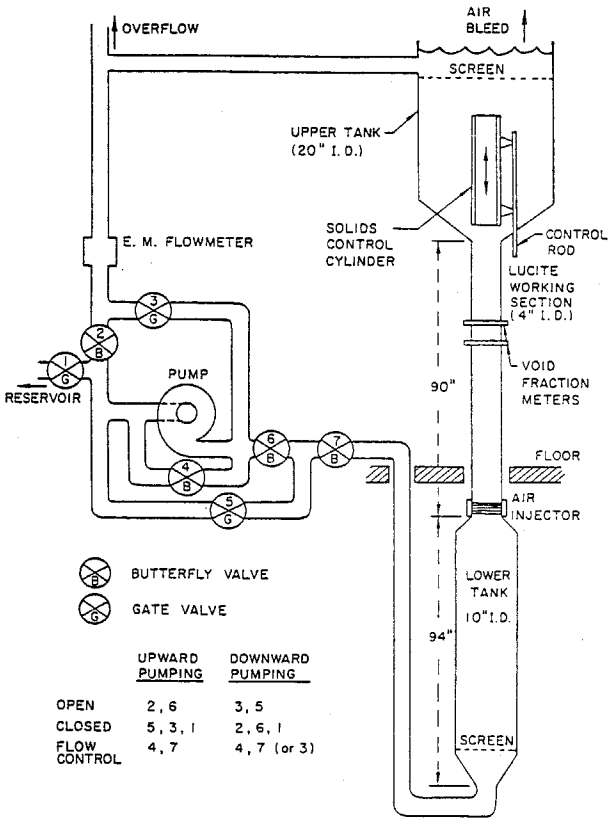

Figure (1) Schematic of the Three Component Flow Facility.

the injector through a regulator, an orifice plate flow meter (to monitor air mass flow), valves to control air flow and a manifold to distribute the air flow evenly among the brass tubes. The solid-liquid flows studied consist of water and polyester particles. The facility is able to handle solids and to control their flow rate independently of the liquid without having to add or remove solids from the exterior of the system. When at rest prior to an experiment the solids are trapped between a vertical 4 inch control cylinder and the storage hopper (see Figure (1)). As the control cylinder is raised from the reducer on top of which it sits, the gap created allows particles to enter the test section under the action of gravity. The vertical position of the control cylinder can be varied by means of a control rod attached to a worm gear mechanism and this permits the solids flow rate to be controlled by varying the gap between the cylinder and the reducer. To recycle the solids after an experiment the control cylinder is lowered to the closed position and sufficient upward water flow is generated to fluidize the solids in the lower tank and to carry them back to the hopper where they settle into their original position.

The volume fraction of the dispersed medium is measured using a non-intrusive Impedance Volume Fraction Meter (IVFM). The IVFM was developed by Bernier (1981). It has been modified for temperature compensation and now has a shielded electrode configuration which decreases the axial extent of the influence volume over which the measurement is carried out. The active stainless steel electrodes which are flush mounted into a section of .1016 meter (4 inch) diameter non-conducting acrylic pipe are 6.4 mm in axial length and form diametrically opposed 90 degree arcs on the circumference of the pipe. The active electrodes are each sandwiched between two shielding electrodes. These are 9.5 mm in axial length and also form 90 degree arcs. Figure (2) shows the electrode configuration. The shielding electrodes duplicate the active electrode potential through a high input impedance voltage follower. The IVFM is excited at an amplitude of .3 volts r.m.s. and a frequency of 40 KHz at which the impedance is found to be primarily resistive. The excitation and signal processing equipment is described in more detail by Bernier (1981), while the shielding and temperature compensation aspects of the device are described in Kytömaa (1986). The IVFM has excellent linearity with both bubbly and particulate flows up to volume fractions of 50%. With a sensitivity of .15 Volts per percent of volume fraction, the passage of individual bubbles (or particles) is readily detectable.

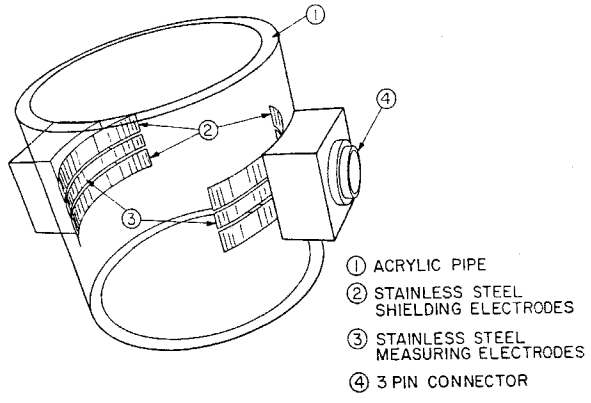

Figure (2) Isometric view of the shielded Impedance Volume Fraction Meter electrode geometry.

The mean bubble and polyester particle diameters were 4 mm (± .5 mm) and 3 mm (± .5 mm) respectively. Only low flowrates were studied; the liquid fluxes of all two-component flows considered were no larger than .3 m/s.

3. THE CROSS-CORRELATION FUNCTION AND ITS INTERPRETATION

It has previously been established that the spatial resolution of the IVFM is of the order of 1 cm in the axial direction (Kytömaa (1986)), and that the influence volume of the measurement remains unchanged for volume fractions and flow rates considered. These properties make the IVFM suitable for the study of volume fraction perturbations over a broad range of wave lengths and allows the IVFM's to be used close to one another without the problem of cross-talk. Measurements of the fluctuations in the volume fraction signal were made simultaneously at two closely spaced locations (h=.0735 m) under steady flow and volume fraction conditions for both bubbly and particulate flows.

The IVFM fluctuating component was obtained by passing the IVFM output signal through a high pass filter with a 3 dB cut off frequency of .032 Hz and a fall off slope of 10 dB per octave. The filter output was recorded on magnetic tape for reduction. The record length used was 1 minute. Cross-correlations of simultaneously recorded data from the two IVFM's were obtained on an HP 3562a signal processor. Repeatable cross-correlograms were obtained by ensemble averaging the measurement with ensembles each of of 1 second in length. The record lengths were as long as 20 minutes for bubbly flow measurements and no shorter than 1 minute in the case of particulate flows. The fluctuating components of the signal pair were cross-correlated to yield the residence time of coherent signal between the two concentration transducers. The cross-correlation ($R_{\tilde{V}_1\tilde{V}_2}$) of the fluctuating components of the two IVFM signals is defined as

$$R_{\tilde{V}_1\tilde{V}_2}(\tau) = \lim_{T\to\infty} \frac{1}{T}\int_0^T \tilde{V}_1(t)\tilde{V}_2(t+\tau)\,dt, \qquad (1)$$

where $\tilde{V}_1$ and $\tilde{V}_2$ are the fluctuations of the IVFM outputs under steady state conditions. Typical measured cross-correlation records are shown in Figure (3). The residence time is obtained from the location in time of the peak in cross-correlograms. Knowing the time taken by the coherent signal to travel from one IVFM to the other, and the distance, h, between the electrode pairs, we calculate the speed of propagation of information, v_X in the two-component flows in question.

$$v_X = \frac{h}{\tau_{max}}, \qquad (2)$$

This propagation velocity is later shown to be the infinitesimal kinematic speed by comparing it with the disperse medium velocities (of bubbles and particles) and the infinitesimal kinematic wave velocities obtained using the Drift Flux Model (Zuber & Staub (1966), Wallis (1969), Kynch (1952)).

Bernier (1981), who used an unshielded IVFM electrode configuration showed that the velocity obtained through cross-correlation was the kinematic wave speed, not the speed of bubbles. At the other extreme, it has been shown that the cross-correlation of the signals of two point volume fraction measuring devices such as hot film anemometers or fiber optic probes separated by a small distance (of the order of the diameter of the dispersed medium) yields the dispersed medium (bubble) velocity. To verify that the speeds measured here are indeed kinematic wave speeds and not the disperse medium speed, we compare cross-correlation speeds to actual bubble and particle speeds and to kinematic wave speeds as predicted by the Drift Flux Model.

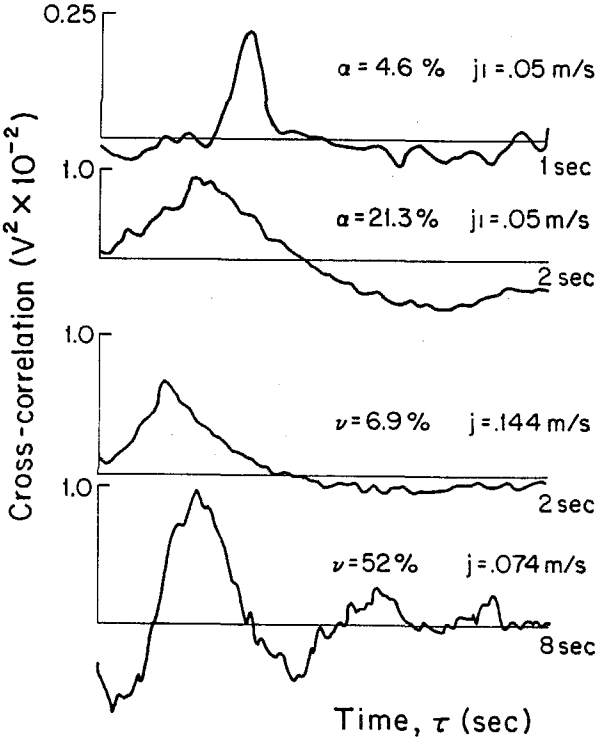

Figure (3) Typical cross-correlations of the IVFM output fluctuating voltage in bubbly and particulate flows.

The bubble speed relative to the liquid is obtained from the measured air and water fluxes (j_g and j_l) and α the volume fraction using

$$v_g = \frac{j_g}{A\alpha} - \frac{j_l}{A(1-\alpha)}. \qquad (3)$$

The kinematic wave speed relative to the liquid is derived using the Drift Flux Model which is well decribed in Wallis's text. It is directly dependent on the relative velocity-volume fraction function obtained experimentally. The Drift Flux infinitesimal kinematic wave speed and the velocity obtained using the above cross-correlation technique are compared in Figure (4). The results eliminate the ambiguity in interpretation of our measurement and

confirms that the cross-correlation of the volume fraction fluctuations (as measured using the IVFM's) yields the speed of infinitesimal kinematic waves for bubbly flows. These findings agree well with similar results obtained by Bouré and Mercadier (1982) who used a capacitive measurement of volume fraction.

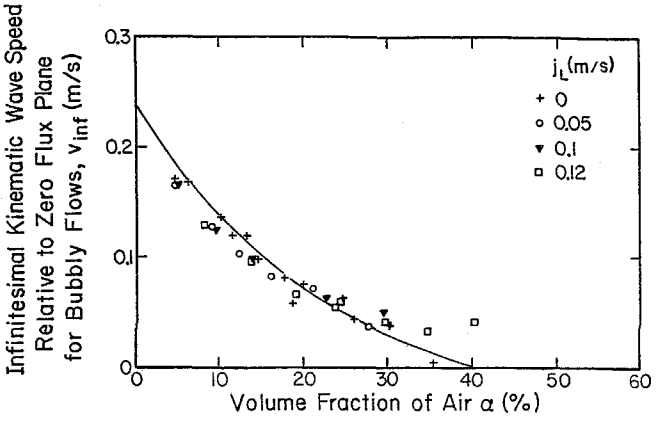

Figure (4) Infinitesimal kinematic wave speed values obtained by the cross-correlation technique for bubbly flows. The solid curve is the infinitesimal kinematic wave speed based on the Drift Flux Model and measurements of the air drift flux.

In polyester particle-water flows we are unable to directly measure the particle speed. The particle velocity relative to water was obtained indirectly by measuring the propagation speed of finite kinematic shocks. This method was tested with bubbly flows and showed to be a consistent method of determining the disperse medium velocity. The method, outlined in detail in Kytömaa (1986), models the particle velocity as the third order function of volume fraction which best fits the kinematic shock speed results. The infinitesimal kinematic wave

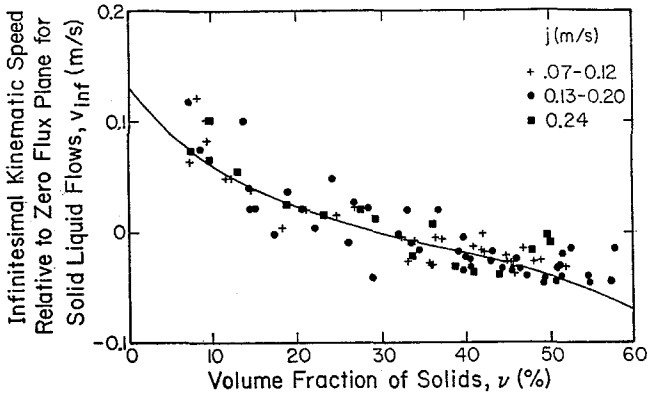

Figure (5) Infinitesimal kinematic wave speed values obtained by the cross-correlation technique for particulate flows. The solid curve is obtained using the Drift Flux Model.

speed obtained from it and the transport velocity deduced from cross-correlation measurements are compared in Figure (5). The results allow us to conclude, as for bubbles, that peaks in the cross-correlation of the IVFM fluctuations for steady polyester particle-water flows correspond to the residence time of infinitesimal kinematic waves between the IVFM's.

4. THE NON-DISPERSIVE NATURE OF INFINITESIMAL KINEMATIC WAVES

In this section we turn our attention to modeling the propagation and attenuation of structure in vertical two-component flows. A measure of the structure is obtained from the statistical properties of the fluctuations in the volume fraction signal. The continuous reordering of the disperse species in the stable steady two-component flows observed is modelled as an attenuation of the coherent signal from one IVFM to the other. The power spectra of volume fraction fluctuations at two different locations of the same (kinematically stable) flow were found to be equal within the scatter in the measurement; experimentally obtained power spectra demonstrate this feature in Figure (6) for two different values of volume fraction for bubbly flows. Therefore, the amplitude of the uncorre-

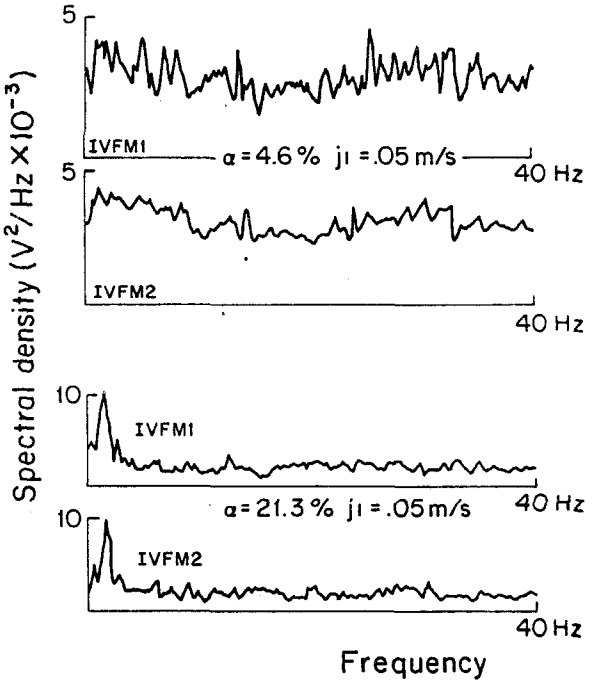

Figure (6) Power spectra of the IVFM output fluctuating voltage measured simultaneously at two locations separated by .0735 m, for bubbly and particulate flows.

lated signal is taken to be equal to the amount removed from the coherent signal through the attenuation, such that the power spectra of the fluctuations of the two IVFM's are the same. In general both the attenuation of the kinematic waves and their residence time between

the IVFM's depend on the wave number. For this reason, the model is best presented in the frequency domain in terms of the wave number of the perturbations. The wave number and the frequency are linearly related by the following expression:

$$N = \frac{\omega}{v_X}. \tag{4}$$

For kinematic waves travelling from IVFM1 to IVFM2, the Fourier-transform of the measured fluctuations can therefore be written as

$$\tilde{\mathbf{V}}_1(N) = \frac{1}{2\pi}\int_{-\infty}^{\infty} e^{-iNt}\tilde{V}_1(t)dt, \tag{5}$$

$$\tilde{\mathbf{V}}_2(N) = \varsigma(N)e^{-iNT(N)}\tilde{V}_1(N) + \tilde{\mathbf{V}}_{2R}, \tag{6}$$

where $\varsigma(N)$ is the wave number dependent attenuation and $T(N)$ is the transit time of the perturbation of wave number N between the two detector positions. The factor $e^{-iNT(N)}$ is the characteristic "time delay exponential" which arises when taking the Fourier- transform of a signal with a time lag $T(N)$. The quantity $\tilde{V}_{2R}$ is the fluctuating term which is not correlated with $\tilde{V}_1$.

The well defined cross-correlation peaks obtained indicate that signal structure propagates at a fixed speed for each record. If the waves were strongly dispersive, the peaks would be broad. Conversely, if the waves were non-dispersive, the peaks would be sharp. Let us first consider the wave number dependence of the delay time. This is best done by studying the phase of the cross-power spectrum of the fluctuations of IVFM1 and IVFM2. This is defined as

$$S_{\tilde{V}_1\tilde{V}_2} = \tilde{\mathbf{V}}_1^*(N)\tilde{\mathbf{V}}_2(N), \tag{7}$$

where * denotes the complex conjugate of the function to which it is applied. Substituting (6) into (7) we obtain

$$S_{\tilde{V}_1\tilde{V}_2} = \varsigma(N)e^{-iNT(N)}S_{\tilde{V}_1\tilde{V}_1}, \tag{8}$$

where $S_{\tilde{V}_1\tilde{V}_1}$ is the power spectrum of the fluctuations of IVFM1, and is defined as

$$S_{\tilde{V}_1\tilde{V}_1} = \tilde{\mathbf{V}}_1^*(N)\tilde{\mathbf{V}}_1(N). \tag{9}$$

Power spectra are real functions; therefore the phase $\phi(N)$ of the cross-power spectrum in (8) is

$$\phi(N) = -NT(N). \tag{10}$$

The cross-power spectrum phase, $\phi(N)$, was evaluated on the signal processor for the recorded data used for the cross-correlation measurements; typical results are shown in Figure (7). The phase was found to be linear in N in the region where the cross-power spectrum amplitude is significant for both bubbly and particulate flows. In other words, $T(N)$ is independent of the wave number N. Thus, the kinematic waves can be considered to be non-dispersive for the range of wave numbers with measurable amplitudes. Therefore the slope of the phase is the time lag of the signal between the two detectors. This was compared to the time lag obtained using the cross-correlation technique. The two were found to be consistent.

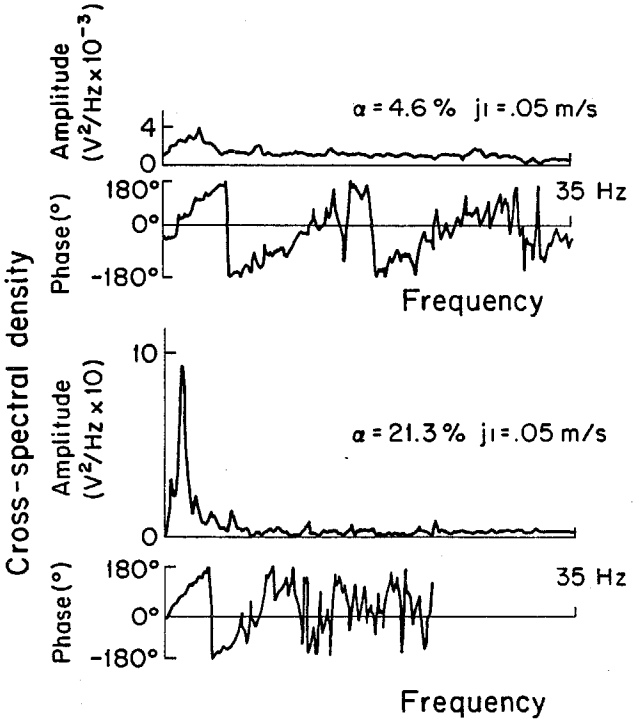

Figure (7) Cross-power spectrum of the IVFM output fluctuating voltage at two locations separated by .0735 m, for bubbly flow showing the linear relation between phase and wave number.

5. THE ATTENUATION OF INFINITESIMAL KINEMATIC WAVES

The main motivation behind shielding the electrodes of the IVFM was to improve the spatial resolution of the device thereby allowing us to study the properties of short wave length infinitesimal kinematic waves ($< .1m$), which have eluded many authors due to the large geometry of their measuring devices. This was successfully accomplished as indicated by the power spectra in Figure (6) which contain reduced wave numbers up to 0.8 or wave lengths down to $.05\,m$.

We now seek the attenuation of infinitesimal kinematic waves as a function of the reduced wave number. This is readily obtained from the coherence function $\gamma(N)$ which is defined as

$$\gamma(N) = \frac{\left|S_{\tilde{V}_1\tilde{V}_2}\right|}{S_{\tilde{V}_1\tilde{V}_1}}, \tag{11}$$

where $\gamma(N)$ can only assume values between 0 and 1. Substituting for $S_{\tilde{V}_1\tilde{V}_2}$ from (7) we get

$$\gamma(N) = \varsigma(N). \tag{12}$$

The attenuation of the correlated signal is identical to the coherence of the fluctuating signals $\tilde{V}_1$ and $\tilde{V}_2$. Assuming that the attenuation is exponential in form, we write

$$\gamma(N) = e^{-k(N)T}, \tag{13}$$

where k is the attenuation time constant of infinitesimal kinematic waves. This form is valid for small fluctuations in the volume fraction signal, which is the case as long as the fluctuations are stable and die away, ie. $k > 0$. Taking the natural logarithm of (13) yields

$$k(N) = -\frac{1}{T} ln\left[\gamma(N)\right]. \tag{14}$$

The attenuation $k(N)$ is always positive since $\gamma(N)$ is always found to be less than 1, as expected since the flows considered here were all invariant with time. The coherence was obtained as a function of wave number from the recordings of IVFM voltage fluctuations on the signal processor. Amplitude resolution of the coherence was enhanced by chosing a relatively broad filter band width (band width: $\Delta n < .0015$) in the frequency domain computation, but narrow enough not to "flatten out" meaningful coherence fluctuations. The coherence displays a "global" maximum at the most persistent wave number which can be seen in Figure (8) for air-water flows and Figure (9) for solid-liquid flows. The attenuation time constant was then deduced using Equation (14) and is shown in Figures (10) and (11) in reduced form against reduced wave number for bubbles and solids respectively.

terminal velocity relative to the continuous medium at zero volume fraction.

6. ERROR ANALYSIS

For all volume fractions of both bubbly and particulate flows, the coherence function exhibits a peak which corresponds to the most persistent wave number. All experimental coherence traces contain some scatter. This is manifested as parasitic non-repeatable fluctuations in the measuerd coherence. This error, which is due to the finite length of our measurements, is inversely proportional to the root of the record length. Clearly, the ideal record length should be very large. However, the batch type particle flows which use a finite volume of particulate material, have a maximum run time which depends on the solids volume fraction and flowrate. The shortest flow duration was one minute. By comparison, twenty minute runs were used for the bubbly flows. The error in coherence is largest in large flow rate, high volume fraction particle flows. However, if the coherence is large then the relative size of the error is decreased. Fortunately, large coherences were obtained for large volume fraction bubbly and solids flows. Since we are most interested in the values of the time constant corresponding to the peak in coherence, the least significant data obtained (low coherence away from the peak) is of little interest to us. The error in the time constant which is algebraically derived from the coherence is

$$\frac{\delta k}{k} = \frac{\delta\gamma}{\gamma ln(\gamma)} + \frac{\delta T}{T}. \tag{16}$$

Based on the scatter in measurements, the error terms

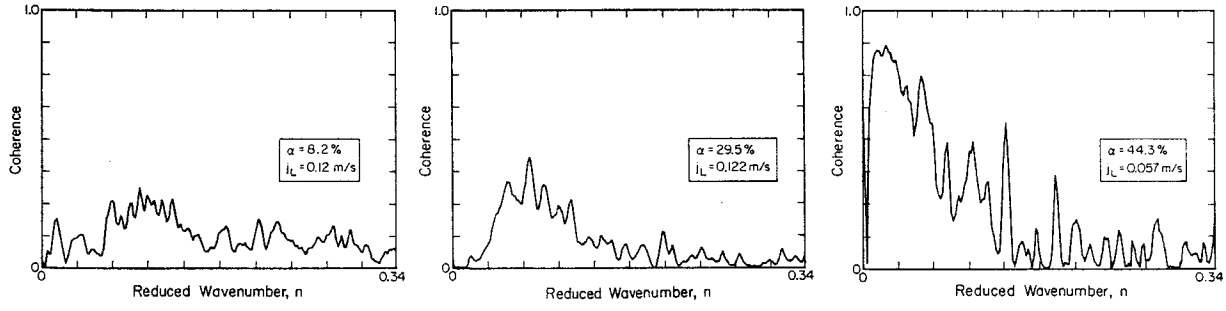

Figure (8) Coherence of the two IVFM fluctuating output signals (separation of IVFM's = .0735 m) in bubbly flows plotted against reduced wave number.

The reduced attenuation time constant and wave number are defined as

$$\kappa = \frac{kD}{V_0}, \quad n = ND. \tag{15}$$

where D is the disperse medium diameter and V_0 is its

are estimated to be:

$$\delta\gamma = .1, \tag{17}$$

and

$$\frac{\delta T}{T} = .2. \tag{18}$$

Using the above, the error in the time constant becomes

$$\frac{\delta k}{k}|_{\gamma=.25} = .49, \tag{19}$$

$$\frac{\delta k}{k}|_{\gamma=.5} = .49, \tag{20}$$

$$\frac{\delta k}{k}|_{\gamma=.75} = .6 \tag{21}$$

The contributions to the error from inaccuracies in the delay time and coherence are found to be of equal order of importance.

7. RESULTS AND DISCUSSION

7.1 TRANSITION FROM BUBBLY TO CHURN-TURBULENT FLOWS

The coordinates of the minimum reduced attenuation time constant, κ and the corresponding wave number n_{min} were noted and each plotted against air volume fraction. A sharp decrease in magnitude of the minimum attenuation constant was measured prior to the change in regime of the air-liquid flow. The minimum reduced attenuation constant κ is shown in Figure (12) versus air volume fraction for bubbly flows. At a volume fraction of 40%, κ starts to decrease abruptly from a value of .03

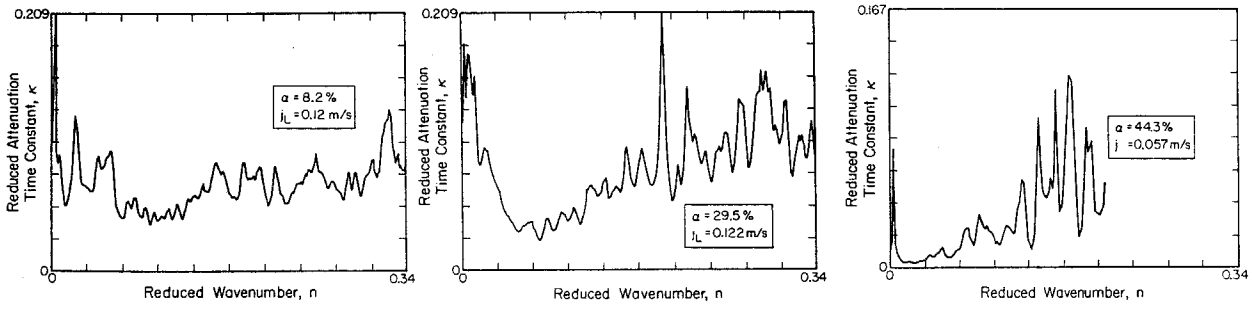

Figure (9) Coherence of the two IVFM fluctuating output signals (separation of IVFM's = .0735 m) in particulate flows.

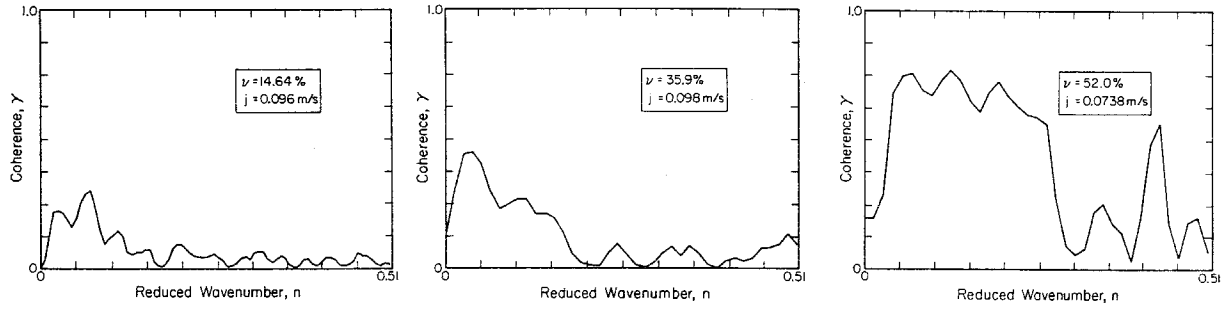

Figure (10) Reduced attenuation time constant calculated from the coherence for bubbly flows, showing a characteristic minimum representative of the least stable wave number. Note the decrease in the minimum value at high volume fraction ($\sim$ 40%) prior to the onset of churn turbulence.

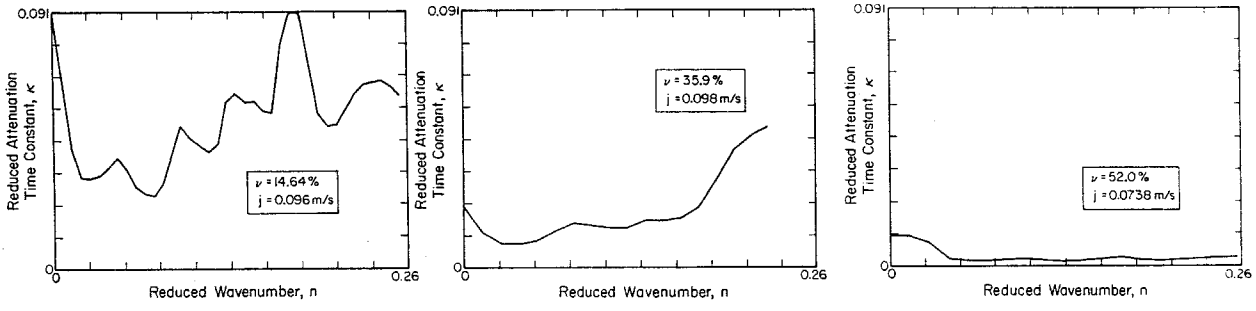

Figure (11) Reduced attenuation time constant calculated from the coherence for particulate flows, showing a characteristic minimum representative of the least stable wave number. Note the broad band decrease in the attenuation time constant at high volume fractions, indicative of the tendency of the medium to conserve its structure.

to less than .003. This sudden fall in κ is accompanied by a shift in the most persistent reduced wave number

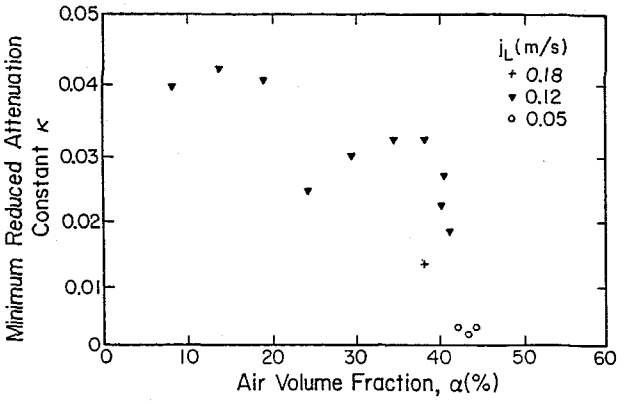

Figure (12) Minimum attenuation constant of bubbly flows of various volume fraction and flow rate conditions presented versus volume fraction. Note the sudden decrease in this variable at $\alpha = 40\%$ prior to the onset of churn-turbulence.

n_{min} from .07 to .03. These values correspond to kinematic perturbation wavelengths of .3m and .8m respectively. These are very large in relation to the pipe diameter which is .1016m. Values of the most persistent wave number n_{min} are plotted in Figure (13). Upon further increase of the air flux the flow becomes churn-turbulent at $\alpha = 45\%$. If we were to extrapolate the experimental κ curve for larger values of volume fraction, κ would cross the horizontal axis at $\alpha \approx 45\%$. Such a change in sign indicates that small perturbations in volume fraction would now grow in an unstable fashion. Thus, the observed onset of large scale structure (churn-turbulence) is interpreted as a loss of kinematic stability.

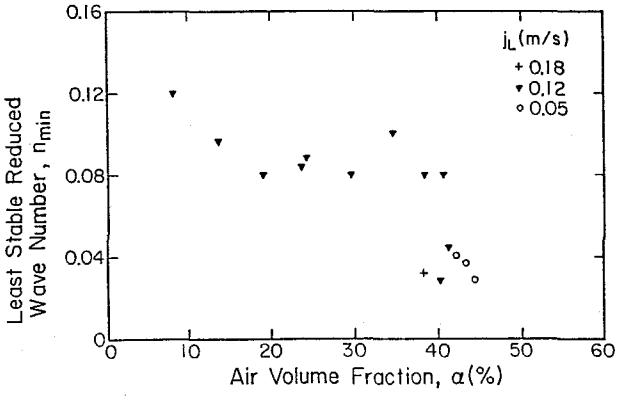

Figure (13) Most coherent wave number in bubbly flows of various volume fractions and flow rates.

7.2 SOLID-LIQUID FLOWS

For solid-liquid flows, the minimum value of the reduced attenuation constant κ of each experiment is plotted against the solid volume fraction in Figure (14) for three groups of total flux. The points describe a curve which has a maximum at $\nu \approx 15\%$. This implies that the mixture loses its structure fastest at this volume fraction. At higher volume fractions (> 15%), the attenuation constant κ for solid-liquid flows gradually decreases from a maximum of .025 to .0015 at $\nu = 55\%$. The monotonic decrease of the minimum attenuation constant for volume fractions > 15% differs from the sudden decrease experienced with the bubbly flows, and it seems to asymptote to the horizontal axis. The bubbly flows, on the other

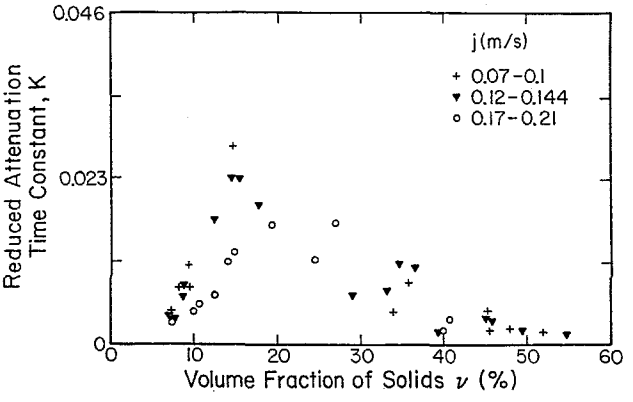

Figure (14) Minimum attenuation constant of particulate flows of various volume fractions and flow rates. The gradually decreasing attenuation constant displays the increased persistence of structure in the flow.

hand exhibited a sharp fall in κ and the subsequent onset of instability as κ became negative. As the extreme case consider a plug flow in which there is no relative motion between particles. For such a flow, the IVFM signals at the two monitoring locations would be identical and exhibit a time lag. The corresponding attenuation constant would then be zero for all wave numbers. The flows considered were not completely plug flows. However, low values (< .003) of κ were obtained for flows with $\nu >= 40\%$. Also, at high volume fractions, the attenuation constant is found to drop to lower values for all wave numbers which is in agreement with the above example. The advent of broad band structure persistence for $\nu > 40\%$ is shown by the sharp increase in the wave number of lowest κ at these high volume fractions in Figure (15). The wave number n_{min} assumes

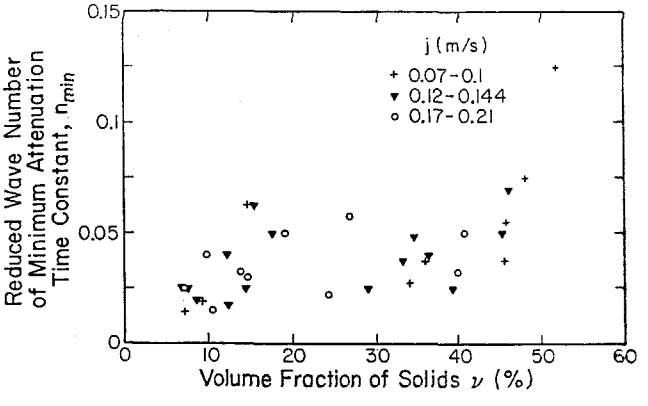

Figure (15) Most coherent wave number in particulate flows of various volume fractions and flow rates.

values of .04 ± .02 for solid fractions up to 40%. The corresponding most persistent wave length in the solid-liquid flows is .5m, which is approximately five time the pipe diameter. In summary, the ability of the particles to withstand particle-particle forces allows the medium to maintain its structure at high volume fractions and no distinct change in flow regime takes place. This is in contrast to bubbly flows of high air volume fraction in which the structure cannot be maintained since close encounters between bubbles lead to coalescence.

8. CONCLUSION

The one-dimensional propagation and attenuation of small amplitude concentration waves in steady state bubbly and particulate flows were measured for the full range of attainable volume fractions. The mixtures studied were initially homogeneously dispersed. The time delay and the decay in amplitude of coherent fluctuations of the volume fraction signal were measured between two closely spaced IVFM's. This information was then used to determine the kinematic wave speed and attenuation as a function of the wave number. The detected waves were determined to be non-dispersive for wave numbers of measurable amplitudes. The wavelength of the most persistent perturbations in volume fraction was of the order of .3 and .5m for bubbly and particulate flows respectively; these dimensions are much larger than the diameter of the pipe (.1m) in which the flows are contained.

The kinematic wave attenuation time constant, κ, was found to be representative of the nature of the flow. In a bubbly mixture, κ began to fall in magnitude at a volume fraction 5% smaller than the critical value at which onset to churn-turbulence occurs. Prior to the change in regime, the structure is increasingly persistent, and ultimately is observed to become unstable. The variable κ was found to behave differently for bubbly and particulate flows. For increasing solids volume fractions, κ assumed slowly decreasing values, and it is shown to reach an asymptotic value of zero corresponding to the translating structure of a plug flow. The smooth decrease in κ corresponds to a gradual transition from the dispersed particulate flow to the plug flow. Despite the persistent structure in solid-liquid flows, these did not exhibit kinematic instability. In contrast, the increased persistence in bubbly flow structure leads to the onset of churn-turbulence.

REFERENCES

1. Anderson, T.B. & Jackson, R., 1967, Ind. Eng. Chem. Fund., Vol. 6, No. 4, p. 527.
2. Anderson, T.B. & Jackson, R., 1968, Ind. Eng. Chem. Fund., Vol. 7, No. 1, p. 12.
3. Batchelor, G.K. and Janse Van Rensbury, R.W., 1986, "Structure Formation in Bi-Disperse Sedimentation", J. Fluid Mech., Vol. 166, pp. 379-407.
4. Bernier, R.N., 1981, "Unsteady Two-Phase Flow Instrumentation and Measurement", Ph.D. Thesis, California Institute of Technology.
5. Bouré, J.A. and Mercadier, Y., 1982, "Existence and Properties of Flow Structure Waves in Two-phase Bubbly Flows", Applied Scientific Research, Vol. 38, pp.297-303.
6. Didwania, A.K. and Homsy, G.M., 1981, "Flow Regimes and Flow Transitions in Liquid Fluidized Beds", Int. J. Multiphase Flow, Vol. 7, No. 6, pp. 563-580.
7. Fessas, Y.P. and Weiland, R.H., 1981, "Convective Solids Settling Induced by a Buoyant Phase", A.I.Ch.E. Journal, Vol. 27, No. 4.
8. Homsy, G.M., El-Kaissy, M.M. & Didwania, A.K., 1980, "Instability Waves and the Origin of Bubbles in Fluidized Beds-
9. Kytömaa, H.K., 1986, "Stability of the Structure in Multicomponent Flows", Ph.D. Thesis, California Institute of Technology.
10. Wallis, G.B., 1969, One Dimensional Two-Phase Flow, McGraw-Hill, New York.
11. Whitmore, 1955,"The Sedimentation of Suspensions of Spheres", Brit. J. Appl. Phys., Vol. 6, pp. 239-245.
12. Zenz, F.A., 1971, Fluidization (editors Davidson J.F. and Harrison, D.), Academic Press.
13. Zuber, N. & Staub, F.W., 1966, "The Propagation of Wave Form of the Vapor Volumetric Concentration in Boiling Forced Convection Systems under Oscillatory Conditions", Journal of Heat Transfer, Vol. 9, pp. 871-895.